A comparative ab initio study of intramolecular proton transfer in model α -hydroxyalkoxides

Rubén D. Parra and Igor Dukarevich

Citation: The Journal of Chemical Physics **122**, 124316 (2005); doi: 10.1063/1.1869474
View online: http://dx.doi.org/10.1063/1.1869474
View Table of Contents: http://scitation.aip.org/content/aip/journal/jcp/122/12?ver=pdfcov
Published by the AIP Publishing

A comparative *ab initio* study of intramolecular proton transfer in model α-hydroxyalkoxides

Rubén D. Parra[a] and Igor Dukarevich
Department of Chemistry, DePaul University, Chicago, Illinois 60614

(Received 14 October 2004; accepted 19 January 2005; published online 30 March 2005)

A comparative *ab initio* study was performed on the intramolecular proton-transfer reaction that occurs in α-hydroxyethanoxy, α-hydroxyphenoxide, and α-hydroxyethenoxy anions. The intramolecular proton transfer occurs in a five-member atom arrangement, between two oxygen atoms separated by a carbon–carbon bond. The chosen systems serve as models for α-hydroxyalkoxide molecules where the carbon–carbon bond varies from a single bond (the glycolate anion or α-hydroxyethanoxide anion) to a part of an aromatic ring (the α-hydroxyphenoxide anion), and finally to a double bond (the α-hydroxyethenoxide anion). Particular attention was given to the evolution along the intrinsic reaction coordinate of such properties as energies, relevant structural parameters, Mulliken charges, dipole moments, and ^{1}H-NMR chemical shifts to reveal the similarities and differences for the proton transfer in the model systems. © *2005 American Institute of Physics*. [DOI: 10.1063/1.1869474]

I. INTRODUCTION

Proton-transfer reactions are one of the crucial processes in biology and chemistry.[1–19] Intramolecular hydrogen bonding interactions are often used as model systems in the study of the proton-transfer reaction.[6,7,12,18,21–27] In addition to providing fundamental insight on the proton-transfer reaction in general, intramolecular hydrogen bonding and the corresponding proton-transfer reaction, where feasible, have been shown to have useful practical applications. Recently, for example, Fukuhara *et al.*,[20] synthesized a planar analog of catechin, a flavonoid molecule, which was shown to be a promising antioxidant with reduced pro-oxidant activity. This planar catechin analog is thought to be useful for the prevention or treatment of free-radical-associated diseases. It was reported that one of the steps involved in the mechanism responsible for the antioxidative and cytoprotective activity of the molecule is an intramolecular proton transfer between the oxygen atoms of the two adjacent hydroxyl groups in the catechin analog. Petrich and co-workers[21] also showed that the naturally occurring polycyclic quinones hypericin and hypocrellin presented strong antiviral and antitumor properties when excited by light. Again, an intramolecular proton-transfer reaction occurring between oxygen atoms attached to the aromatic rings of hypericin and hypocrellin is found to play a key role in the function of these potentially useful molecules. An understanding of the intramolecular proton transfer in these and other complex cases may be first gained by studying simpler, more manageable model systems. *Ab initio* studies in simpler systems provide detailed information such as energies, geometries, vibrational frequencies, and electronic charge redistribution. This information is essential to further our knowledge of the process, yet it is often difficult, even impossible in some cases, to obtain such information experimentally.

It is particularly appealing that in many biochemically important processes, such as the one in the planar catechin analog mechanism,[20] the intramolecular proton transfer occurs in a five-member atom arrangement, between two oxygen atoms separated by a carbon–carbon bond, and with an overall negative charge localized mainly on one of the oxygen atoms. It is of basic interest then to investigate this type of proton-transfer reaction in appropriate model systems. Fairly recent comparative *ab initio* studies have been performed on proton transfer in similar types of five-member rings. Scheiner *et al.*[22] studied intramolecular proton transfer in ground and exited states of anionic analogs of malonaldehyde. Their work focused mainly on expanding the ring involved in the transfer, from five to seven atoms, and in which the system bears an overall negative charge. Bosch *et al.*[23] reported a comparative *ab initio* study of proton transfer in the glycolate, hydroxyacetate, and hydrogenoxalate anions. They analyzed the energetics, intrinsic reaction coordinate (IRC), and electron density rearrangement during the transfer. Bertran and co-workers[24] investigated the effect of ionization on the intramolecular proton-transfer process on the glycine radical cation. Other theoretical studies have focused specifically on the intramolecular proton transfer in the glycolate anion as a test case. These studies include the calculation of the minima and the transition state geometries and the height of the barrier to proton transfer,[25] and the assessment of different methods to study direct tunneling dynamics.[26,27] In this work, we have investigated the intramolecular proton transfer in three model systems of α-hydroxyalkoxides. More specifically, we have conducted a systematic comparison of the proton transfer that occurs in α-hydroxyethanoxy, α-hydroxyphenoxide, and α-hydroxyethenoxy anions. In these model systems, the intramolecular environment surrounding the five-membered

[a]Author to whom correspondence should be addressed. Electronic mail: rparral@depaul.edu

ring involved in the proton transfer is varied systematically. For example, the carbon–carbon bond of the ring varies, respectively, from a single bond to a part of an aromatic benzene ring, and finally to a double bond. The basic scheme for these possibilities is presented in Fig. 1. The evolution along the IRC of such properties as energies, reaction forces, relevant structural parameters, Mulliken charges, dipole moments, ^{1}H-NMR chemical shifts, and chemical potentials was used to reveal the similarities and differences for the proton transfer in the three model systems.

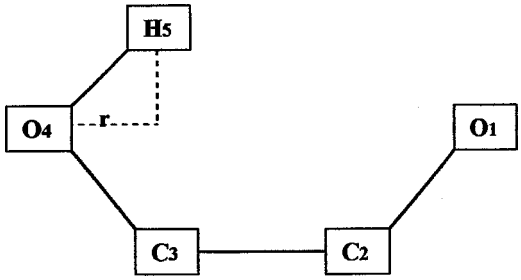

FIG. 1. Schematic representation of the five-atom arrangement for the proton-transfer reaction in the model α-hydroxyalkoxide systems considered in this work.

II. METHODS

Ab initio calculations were performed with the GAUSSIAN 2003 program package.[28] Geometry optimization, frequency calculations, and IRC calculations were carried out at the MP2/6-31+G(d,p) level of theory. The so optimized geometries were used to obtain single point energies along the reaction coordinate at the QCISD, MP4, MP2, and Hartree–Fock (HF) levels with the 6-31++G(d,p) basis set. NMR chemical shifts were calculated at the B3LYP/6-311+G($2d,p$) level using the gauge-independent atomic orbital method, as found in the GAUSSIAN 2003 program.

III. RESULTS AND DISCUSSION

The following convention is followed: *single* refers to α-hydroxyethanoxide, also known as the glycolate anion, where the carbon–carbon bond (C_3-C_2 in Fig. 1) is a single bond; *aromatic* refers to α-hydroxyphenoxide where the carbon–carbon bond is part of the aromatic benzene ring; *double* refers to α-hydroxyethenoxide where the carbon–carbon bond is a double bond.

A. Equilibrium geometries and barriers to proton transfer

Table I lists the chief geometric parameters of the reactants R and their corresponding transitions states (TS). Also shown in Table I are the geometrical changes as the systems move from reactants to transition states. Since the reactants are simply mirror images of the products, only reactants are discussed. The barriers to the proton-transfer process are presented in Table II at different levels of theory. The results shown in Table II indicate that the HF method consistently overestimates the barrier heights compared with the correlated methods used in this study. This overestimation has been explained in terms of the dispersion interactions whose description is missing at the HF level.[3,22–27,29,30] Dispersion interactions are accounted for by means of correlated methods such as MP2, MP4 and QCISD. Although the MP4 and QCISD results are close to each other, the MP2 barriers are consistently lower indicating an overcorrection to the HF values.[27]

The trends in the proton-transfer barriers may be rationalized in terms of the strength of the hydrogen bond present in the reactants.[2,18,22] A relatively strong hydrogen bond should correlate with a long O–H bond distance, a short O···O separation, and a small O···O–H angle. It is apparent (Table I) that the strength of the hydrogen bond in the reactants follows the order single > aromatic > double. As expected, this order opposes that of the barrier heights. In general, the extent of geometrical distortions follows the order double > aromatic > single in accord with the trends of the barrier heights. Major changes are observed for the O1–H5 and the O···O distances for all systems.

Because the proton transfer requires a reordering of both

TABLE I. Relevant MP2/6-31+G(d,p) optimized structural parameters.

	Reactants			TS			TS reactants		
Lengths (Å)	Single	Aromatic	Double	Single	Aromatic	Double	ΔSingle	ΔAromatic	ΔDouble
C3–O4	1.426	1.377	1.412	1.400	1.339	1.364	−0.026	−0.038	−0.048
C2–O1	1.374	1.304	1.311	1.400	1.338	1.364	0.026	0.034	0.052
C3–C2	1.551	1.441	1.370	1.569	1.441	1.371	0.018	0.000	0.000
O4–H5	1.013	0.995	0.982	1.229	1.242	1.245	0.216	0.247	0.262
O1–H5	1.713	1.852	2.046	1.229	1.243	1.246	−0.484	−0.609	−0.801
O4–O1	2.527	2.582	2.712	2.347	2.351	2.359	−0.180	−0.231	−0.353
Angles (°)									
C2–C3–O4	106.0	113.4	116.6	104.6	109.9	111.2	−1.4	−3.6	−5.4
C3–C2–O1	108.4	117.0	122.5	104.6	109.9	111.2	−3.8	−7.1	−11.3
C3–O4–H5	96.0	98.9	99.2	89.9	89.0	87.5	−6.1	−9.9	−11.7
C2–O1–H5	84.1	83.0	78.4	89.9	89.0	87.5	5.9	5.9	9.0
O1–O4–H5	29.1	34.6	39.2	17.3	18.9	18.7	−11.8	−15.7	−20.4
O4–C3–C2–O1	−37.5	1.8	−0.1	−24.9	1.7	0.0	12.5	−0.1	0.1
H5–O4–C3–C2	24.5	−1.4	0.0	17.3	−1.1	0.0	−7.3	0.2	0.0

TABLE II. Electronic potential energy barriers (kcal/mol) obtained using the 6-31++G(d,p) basis set and the MP2/6-31+G(d,p) optimized geometries.

Method	Single	Aromatic	Double
HF	6.45	11.26	17.37
MP2	2.07	4.70	7.37
MP4	3.47	6.64	9.90
QCISD	3.63	6.74	10.06

the molecular geometry and electron density, it is evident that a proton transfer in which a double bond is involved near the backbone structure will need more energy and present the most significant distortions. A reordering of the electron density is manifested, for example, in changes of the dipole moments. At the QCISD/6-31++G(d,p) level, the calculated changes are −0.33, 0.11, and 0.23 D for single, aromatic, and double, respectively. Consequently, the work of charge separation upon half transfer of the proton should be large in double which contributes to its large proton-transfer energy barrier. In comparison, the low barrier in single can be attributed in part to the overall reduction of its dipole moment. In aromatic, the π-electron resonance of the aromatic ring provides a partial compensation of charge redistribution resulting in a dipole moment increase lower than that in double which lacks such intramolecular compensation. In addition to the dipole moment, a powerful tool that may be used to discuss electronic redistribution is the chemical potential μ which, within the framework of density functional theory,[31] characterizes the escaping tendency of electrons from the equilibrium system. An approximate value of μ at a given point in the reaction coordinate is normally obtained by using the equation

$$\mu = \tfrac{1}{2}(\varepsilon_L + \varepsilon_H),$$

where ε_H and ε_L are the energies of the highest occupied molecular orbital (HOMO) and lowest unoccupied molecular orbital (LUMO), respectively.[6,7] The changes in chemical potential are −8.10, −2.52, and −1.07 kcal/mol for the single, aromatic, and double systems, respectively. The negative sign indicates that for each system electrons flow from the reactant (high μ) toward the transition state (low μ). It is clear that positioning the proton in the TS geometry benefits from the simultaneous flow of electrons toward the TS. The relatively small changes in μ for double and aromatic help explain their high proton-transfer barriers compared with single.

B. Geometry, energy, and force profiles

Valuable information on the proton-transfer mechanism can be obtained by following the evolution of relevant geometrical parameters along the reaction path. To this end, we have calculated the IRC for all the systems at the QCISD/6-31++G(d,p) level. In this study, we monitor the evolution of the O···O and the O4–H5 bond distances as the proton-transfer progresses along the IRC. More specifically, we follow the evolution of the O4–H5 elongation and the O···O contraction taking the TS geometry as the reference

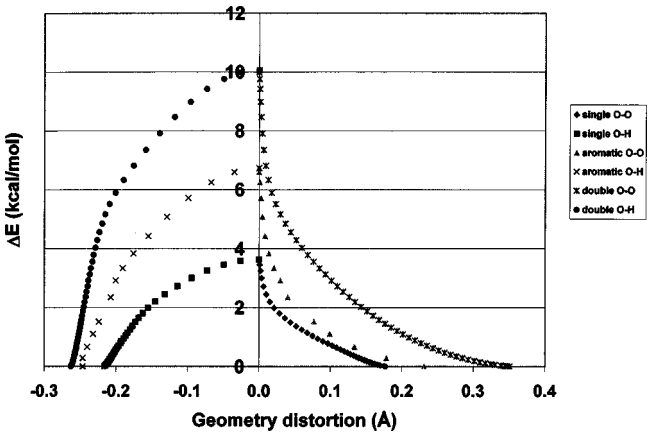

FIG. 2. Relative energies vs O···O and O4–H5 distortions along the IRC coordinate from reactant to TS.

point. The results are exhibited in Fig. 2. Clearly the reaction from the reactant to the transition state proceeds in two very distinct steps. The first step is largely dominated by the O···O distance contraction while H5 moves apart from O4 only slightly. The second step is largely dominated by the O4–H5 elongation with no change in the O···O. The first step requires ≈2.4 kcal/mol (67%), 4.4 kcal/mol (66%), and 6.8 kcal/mol (68%) for single, double, and aromatic, with the values in parentheses indicating the percentage of the pertinent barrier heights.

The geometry profiles can be rationalized in terms of the reaction force profiles. Quite recently Toro-Labbe and co-workers[32,33] have shown that the reaction force profile of a chemical reaction following the intrinsic reaction coordinate, F(IRC), is a powerful tool to characterize the reaction mechanism. Regions along the reaction coordinate where different steps of the reaction mechanism operate can be distinguished in terms of the reaction force profile. In this study, we have calculated the reaction force along the IRC to enhance the physical-chemical rationalization of the proton-transfer reaction in the model α-hydroalkoxides systems considered. To this end, the QCISD/6-31++G(d,p) potential energy profiles along the IRC for the systems were first obtained and the results are shown in Fig. 3. The so obtained energy profiles were used to compute the corresponding force profiles and the results are displayed in Fig. 4. The forces F are obtained as the negative of the numerical differentiation of the potential energy with respect to the reaction coordinate.[32,33] Two critical points, a minimum and a maximum, are observed for each force profile. The numerical values of force and IRC for these critical points are the same by symmetry. The work necessary to bring the systems from the reactants geometry to the geometry adopted at the minimum point is calculated by integration of the force from $-\infty$ to the position of the minimum. The work required to reach the TS geometry from the minimum point is likewise calculated from the minimum to IRC=0 and the results are shown in Table III. In all cases there is a considerable amount of energy that is used to bring the systems into proper geometry before the proton is allowed to reach its final position in the TS. In fact, the work needed for the first step accounts for 75% (single), 67% (aromatic), and 79% (double) of the total

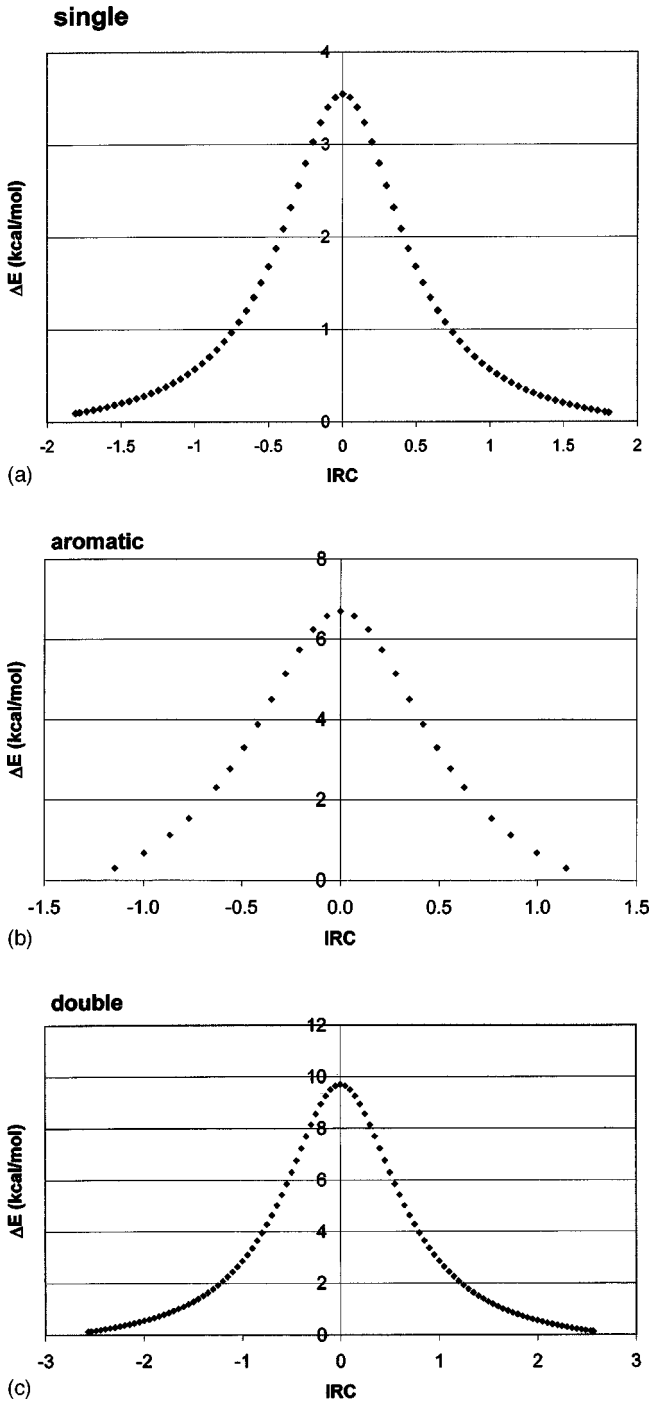

FIG. 3. QCISD/6-31++G(d,p)//MP2/6-31+G(d,p) energy profile for single, aromatic, and double.

energy barrier. These values are close to those found for the related O···O contractions. Thus, the reaction force profiles along with Fig. 2 allow us to rationalize the reaction mechanism as a two-step process. In the first step, the donor and acceptor oxygen atoms get close enough to facilitate the transfer of the proton necessitating most of the energy barrier; in the second step, the proton moves now to its position in the TS geometry requiring less energy and the reaction keeps going on until it reaches the configuration of the product.

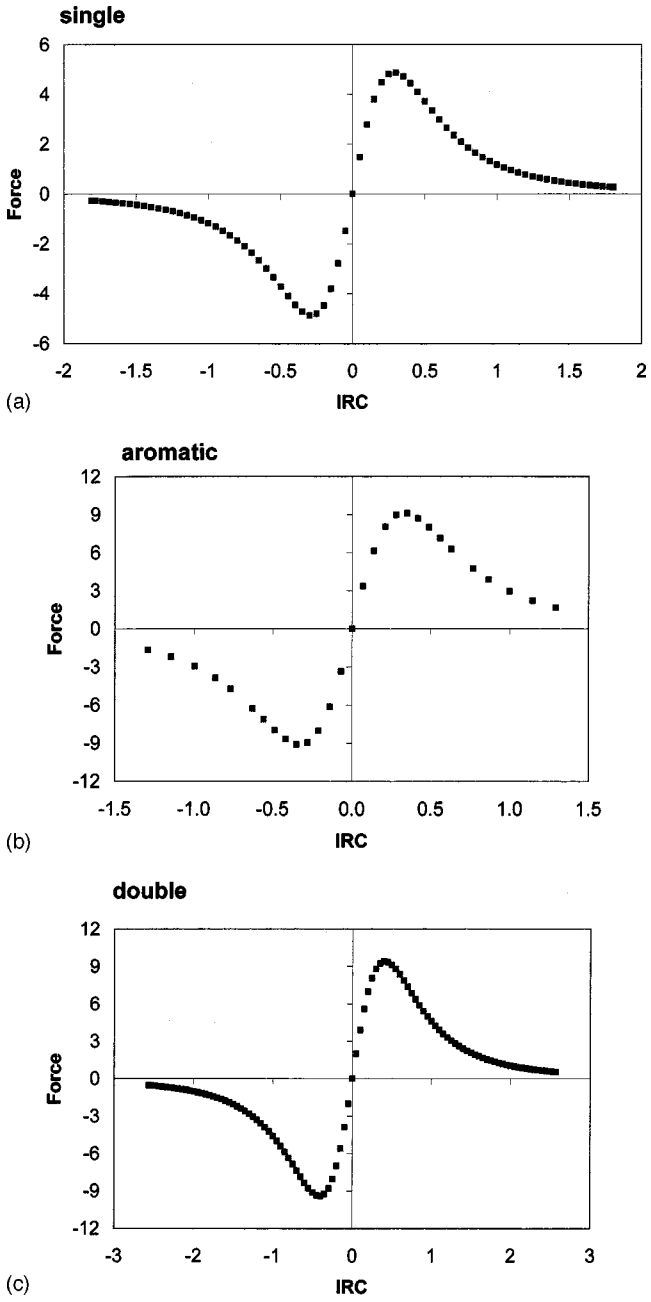

FIG. 4. Reaction force profile for single, aromatic, and double.

C. Mulliken charge and dipole moment profiles

Table IV shows the respective Mulliken charges of the O4, H5, and O1 atoms for the reactants and transition states. The evolution of the charge changes along the IRC are dis-

TABLE III. QCISD/6-31++G(d,p)//MP2/6-31+G(d,p) minimum position in the reaction force profile, work done by the system to bring the oxygen atoms close to each other ($|W_a|$), and work associated with the hydrogen moving toward its TS configuration $|W_b|$.

System	Minimum[a]	$\lvert W_a\rvert$	$\lvert W_b\rvert$
Single	−0.249 (86%)	2.72	0.91
Aromatic	−0.349 (73%)	4.54	2.19
Double	−0.300 (88%)	7.91	2.15

[a]Values in parentheses indicate the percent IRC completion toward TS.

TABLE IV. Mulliken charges q, dipole moments (DM), absolute proton chemical shifts δ, and chemical potentials μ calculated using the MP2/6-31+G(d,p) geometries.

	Reactants			TS			TS reactants		
Property[a]	Single	Aromatic	Double	Single	Aromatic	Double	ΔSingle	ΔAromatic	ΔDouble
q_{O1} (a.u.)	−0.941	−0.874	−0.8872	−0.860	−0.801	−0.8186	0.081	0.073	0.069
q_{O4} (a.u.)	−0.703	−0.643	−0.641	−0.860	−0.804	−0.8186	−0.158	−0.161	−0.178
q_{H5} (a.u.)	0.415	0.425	0.391	0.498	0.494	0.498	0.083	0.069	0.107
δ (ppm)	23.47	22.54	26.39	16.38	13.07	13.25	−7.08	−9.47	−13.14
DM (D)	3.874	4.122	2.381	3.543	4.237	2.609	−0.331	0.115	0.228
μ(kcal/mol)	5.44	14.06	29.42	−2.66	11.53	28.35	−8.1	−2.53	−1.07

[a]Chemical shifts obtained at the B3LYP/6-311+G(2d,p) level. All other properties calculated at the QCISD/6-31++G(d,p) level.

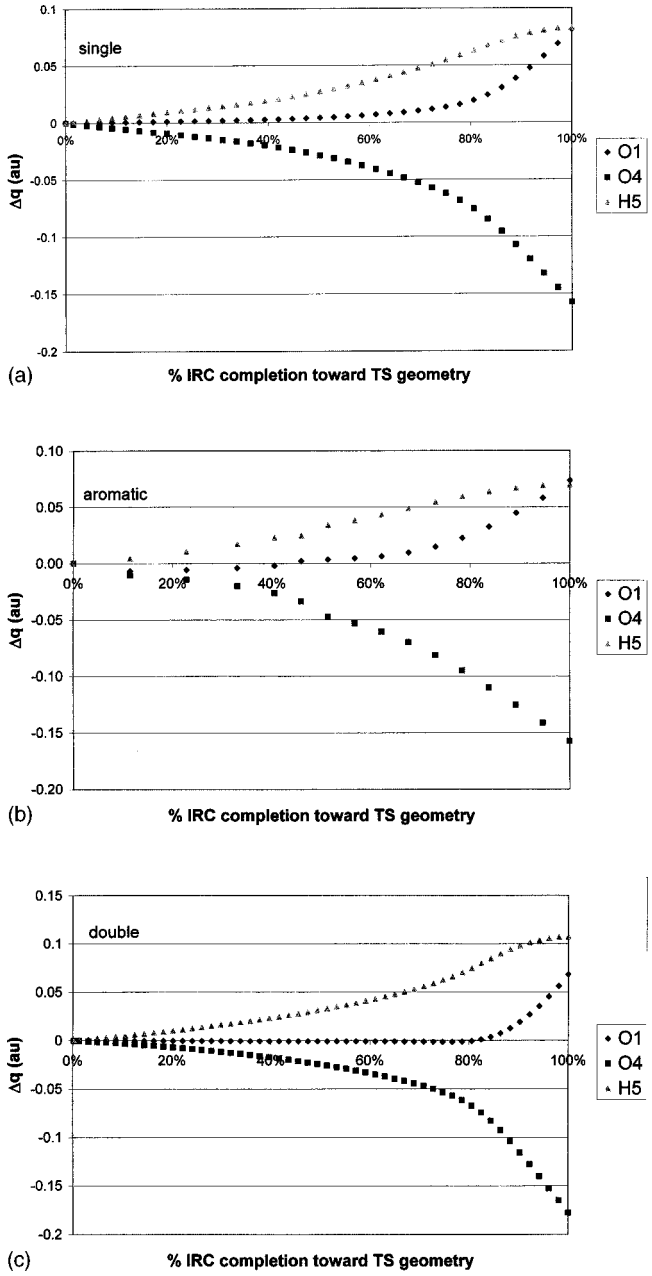

FIG. 5. Change in Mulliken charges along the IRC from reactant to TS for single, aromatic, and double.

played in Fig. 5. The charge changes are displayed as a function of the percentage of the IRC completion toward TS. There is a net gain of electron density in the proton-donor oxygen atom (O4) almost compensated by the loss of electron charge seen in both the proton-acceptor oxygen atom (O1) and the bridging hydrogen atom (H5). One striking feature observed in Fig. 5 for all systems is that the rates of change in the charges of the three atoms differ greatly. Thus for any given system, the rates of change of the O4 and O1 charges remain relatively small, even negligible in the case of the O1 atom, until they increase notoriously at a point along the IRC that coincides or it is very close to that of the minimum found in the corresponding reaction force profile. The opposite behavior is seen for the rates of change of the proton in all systems. For example, a substantial increase in the rates of change of the oxygen atom charges, accompanied by a drop in the rate of charge change of H5, occurs in the double system at about 85% of the IRC. This position along the IRC is very close to the 88% value corresponding to the minimum in the corresponding force profile.

Table IV lists the dipole moments for the reactants and transition states. The changes in dipole moment, along the intrinsic reaction coordinate, resulting from half transfer of the proton in the three systems are displayed in Fig. 6. While a net reduction in the dipole moment is observed for the single system, the opposite is true for the other two systems. The consequence of this on the height of the barrier for the transfer of the proton in the systems was discussed early in

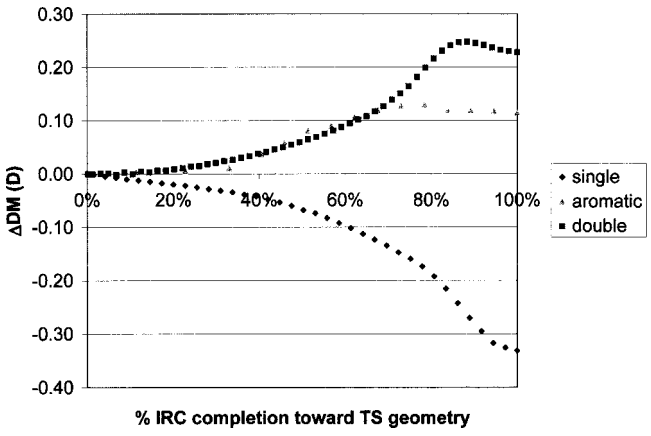

FIG. 6. Change in dipole moment (DM) along the IRC from reactants to TS.

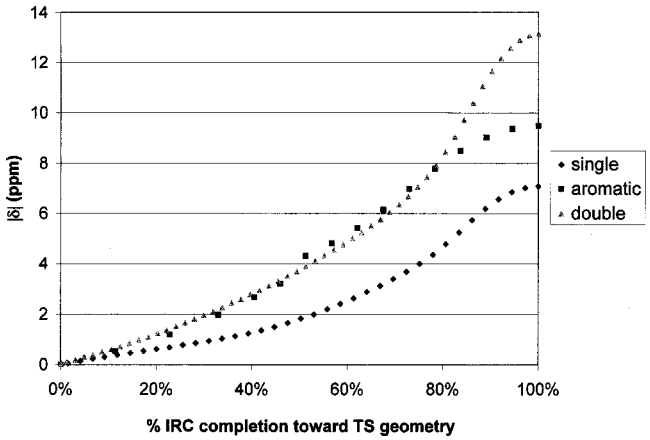

FIG. 7. Absolute changes in ^{1}H chemical shift along the IRC from reactants to TS.

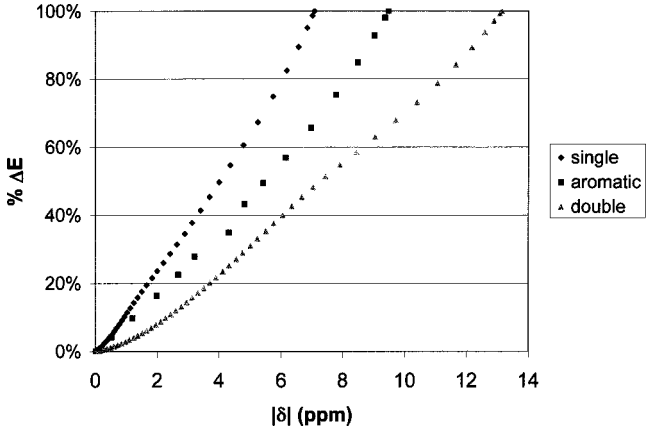

FIG. 8. Percent energy change vs absolute ^{1}H chemical shift change along the IRC from reactants to TS.

this paper. Simultaneous inspection of Fig. 5 and 6 shows that the changes in dipole moment correlate well with the corresponding changes in the charges of the two oxygen atoms and the proton being transferred. Thus, the rates of change in the dipole moments are significantly altered at points along the IRC close to those found for the corresponding minima in the reaction force profiles of the systems. It is apparent that for any given system the loss of electron density on O1, which begins at a point along the IRC close to the minimum in the reaction force profile, results in a reduction of dipole moment leading to the leveling off of the dipole moment changes for aromatic and double, and to an even greater reduction in the dipole moment for single until it levels off to its value in the TS geometry. Our results are consistent with those of Herrera and Toro-Labbe[33] who also observed in the systems they studied that the most noticeable changes in the Mulliken electron populations and dipole moments along the IRC occur within the region defined by the critical points of the force profiles.

D. ^{1}H-NMR profiles

An important spectroscopic technique that has shown great potential in investigating the strength of a hydrogen bond is NMR.[34–38] Because the strength of the intramolecular hydrogen bond interaction influences the energy of the proton-transfer reaction, we have studied the evolution of the ^{1}H-NMR chemical shifts δ for the H5 atom, relative to its value in the reactant form, from the reactant to the transition structure along the IRC. The chemical shifts for the reactants and transition states are shown in Table IV. The results for the evolution of the chemical shifts in the three systems are displayed in Fig. 7, where for convenience we have chosen to display the absolute values of the relative changes in the chemical shifts for the H5 atom. The largest overall change is for double ($|\Delta\delta|=13.14$ ppm), whereas the smallest change is for single ($|\Delta\delta|=7.08$ ppm). The net change in the aromatic system ($|\Delta\delta|=9.47$ ppm) falls almost half between those of the other two systems. Figure 7 shows that although the evolution profile of the changes in chemical shifts along the IRC follows a similar qualitative pattern in all three systems, the single system curve separates notoriously from the others at about 10% completion of the IRC. The curves for the aromatic and double systems remain close to each other up to about 80% completion of the IRC. The respective ^{1}H-NMR chemical shift changes begin to slow down at about 90% IRC for single and double, and at about 80% IRC for aromatic. Again, the IRC values are close to the pertinent minima in the reaction force profiles. The ^{1}H-NMR results parallel those for the relative H5 charge change observed in Fig. 3. A reduction in the proton charge change should result in a comparatively less deshielded proton which in turn leads to a small chemical shift change.

A convenient plot of the percent of the proton-transfer energy barrier versus the absolute change in ^{1}H-NMR chemical shift is exhibited in Fig. 8, which shows a clear separation of the three curves while maintaining a fairly linear relationship between the plotted parameters. It should be mentioned that even though plotting the energy change, as opposed to the percent energy change, versus the absolute changes in ^{1}H-NMR chemical shift also results in a linear relationship for each system, the aromatic and double system curves have the same slope and are therefore hard to tell apart.

E. Chemical potential μ profiles

The profiles of the changes in μ, relative to reactants and calculated with the HOMO and LUMO energies as discussed previously, are illustrated in Fig. 9. It is seen that the μ changes strongly along the IRC for single, while only small changes are seen for aromatic and double. For all systems, almost half of the overall μ changes are accounted for by the rearrangements of electron density as the systems move from reactants to the vicinity of the IRC minima in the reaction force profiles. Then, the rates of change in μ present a sizeable increase, particularly for single, until they level off to their final values. These results are consistent with the electron density redistribution as reflected for example in the dipole moment and Mulliken charge changes (Fig. 5 and 6). It is important to highlight that as the proton moves from its position in the reactant to that in TS, the electron density of O4 decreases whereas that of O1 increases indicating that there is charge transfer in the opposite direction to the mo-

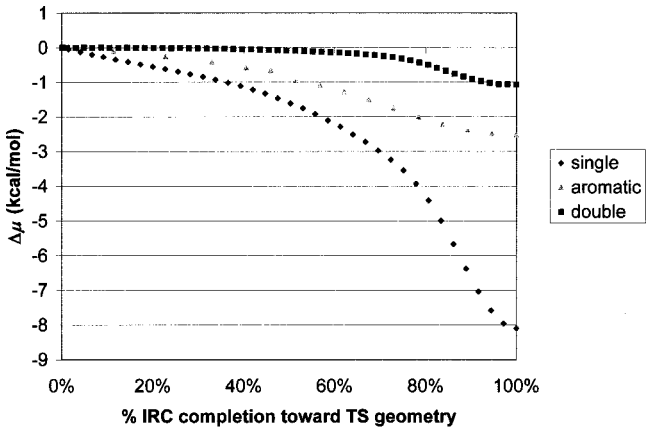

FIG. 9. Changes in chemical potential μ along the IRC from reactants to TS.

tion of the proton. Since electron transfer is driven by chemical potential differences, we would expect considerable electron transfer, a large change in the O4 and O1 Mulliken charges, within regions of large μ differences. This fact is easily verified by simultaneous inspection of Figs 6 and 8. Moreover, the qualitative ordering of the μ changes correlates well with the qualitative ordering of the barrier heights. Therefore, the larger the μ differences, the easier it is for the proton acceptor oxygen atom to transfer electron to the proton donor oxygen atom, and then the lower the barrier to the proton transfer.

F. Analytical functions for the proton-transfer potentials

The proton-transfer potentials for the systems computed at the QCISD/6-31++G(d,p) level along their IRC were fit to the following fourth-order polynomial functions[39]

$$\Delta E = \varepsilon\{(r/u_o)^2 - 1\}^2 \tag{1}$$

and

$$\Delta E = Ar^4 + Br^2 + C. \tag{2}$$

In these functions, r is the projection of the O4–H5 bond length along the O$\cdots$O axis (Fig. 1). For fitting purposes, r is taken relative to its value in the TS geometry. Two fitting possibilities, fitting A and fitting B, respectively, were considered for each function depending on the number of parameters used. In fitting A, two parameters ε and u_o were used for function 1 [Eq. (1)], whereas three parameters, A, B, and C were used for function 2 [Eq. (2)]. In fitting B, the parameters ε and C for functions 1 and 2, respectively, were assigned the values of the barrier heights for each model system and kept constant. By doing so, the number of parameters to optimize is decreased by 1. The fitting parameters are listed in Table V. The quality of fitting is quite respectable for both functions and for all three systems as evidenced by the correlation parameter $R^2 = 0.981$ or better. It is also encouraging to see that fixing one parameter, fitting B, does not alter the quality of fitting to any considerable extent. However, although the constant parameter C in Eq. (2) may be made to correspond to the electronic energy barrier to the proton transfer, the values of the parameters A and B are quite sensitive. In contrast, the parameters for Eq. (1), ε and u_o, show some relationship with the C3–C2 bond order. For convenience, we can assign bond orders of 1.0, 1.5, and 2.0 for the single, double, and aromatic systems. By doing so, a direct relationship exists between the parameter ε and the C3–C2 bond order. A quadratic relationship is found between the values of u_o and the C3–C2 bond order. We can then in principle predict the energy profile of the proton transfer in similar systems with differing C3–C2 bond orders. Additional model studies should reveal whether these findings represent general trends.

IV. SUMMARY

A comparative *ab initio* study has been conducted on the intramolecular proton-transfer reaction occurring in three model α-hydroxyalkoxides denoted single, aromatic, and double based on the C–C bond order of the near backbone structure (Fig. 1). It is found that the barrier to proton transfer increases linearly with the C–C bond order. The QCISD/6-31++G(d,p) barriers are 3.63 kcal/mol (single), 6.74 kcal/mol (aromatic), and 10.06 kcal/mol (double). The ordering of the barrier heights follows from the rearrangement of both the molecular geometry and the electron den-

TABLE V. Fit of parameters to two polynomial functions to QCISD/6-31++G(d,p) *ab initio* proton-transfer potentials.

Function 1[a]	Fitting A			Fitting B		
Parameters	Single	Aromatic	Double	Single	Aromatic	Double
ε (kcal/mol)	3.86	6.73	10.59	3.63	6.74	10.06
U_o (A)	0.319	0.396	0.443	0.325	0.396	0.449
R^2	0.986	0.997	0.989	0.981	0.997	0.985
Function 2[b]						
A (kcal mol^{-1} A^{-4})	193.404	230.700	211.055	155.406	240.422	183.984
B (kcal mol^{-1} A^{-2})	−62.368	−82.009	−98.213	−58.351	−83.554	−92.049
C (kcal mol^{-1} A^{-1})	3.72	6.69	10.37	3.63	6.74	10.06
R^2	0.995	0.999	0.993	0.994	0.998	0.992

[a]$\Delta E = \varepsilon.(r/u_o)^2 - 1)^2$.
[b]$\Delta E = Ar^4 + Br^2 + C$. r is the projection of the O4–H5 distance along the O$\cdots$O axis.

sity. A proton transfer for double requires the most geometry distortions which results in its having the largest proton-transfer barrier. Electron redistribution as reflected in changes in dipole moment and chemical potential also helps rationalize the ordering of the barrier heights. The reaction force profile along the reaction coordinate proves to be a compelling means to characterize the mechanism of proton transfer.[32,33] The analysis of the evolution of such properties as Mulliken charges, dipole moments, and chemical potentials shows that the major changes along the IRC appear nearby the first critical point indicated by the force profiles. Finally, simple analytical functions for the modeling of the proton-transfer reaction in similar systems with differing C–C bond order are provided.

ACKNOWLEDGMENTS

This research was funded by a Faculty Research and Development grant at DePaul University, and by an Alexandroff summer research grant from the DePaul University Chemistry Department.

[1]E. F. Caldin and V. Gold, *Proton-Transfer Reactions* (Chapman and Hall, San Francisco, CA, 1975).
[2]A. Koll, Int. J. Mol. Sci. **4**, 434 (2003).
[3]S. Scheiner and L. D. Bigham, J. Chem. Phys. **82**, 3316 (1985).
[4]D. Wei, J. Truchon, S. Sirois, and D. Salahub, J. Chem. Phys. **116**, 6028 (2002).
[5]S. Yen, C. Lin, and J. Ho, J. Phys. Chem. A **104**, 11771 (2000).
[6]E. Chamorro, A. Toro-Labbe, and P. Fuentealba, J. Phys. Chem. A **106**, 3891 (2002).
[7]B. Herrera and A. Toro-Labbe, J. Phys. Chem. A **108**, 1830 (2004).
[8]M. A. Lill, M. C. Hutter, and V. Helms, J. Phys. Chem. A **104**, 8283 (2000).
[9]D. Alfano, R. Borrelli, and A. Peluso, J. Phys. Chem. A **106**, 7018 (2002).
[10]B. Schiøtt, B. B. Iversen, G. K. H. Madsen, F. K. Larsen, and T. C. Bruice, Proc. Natl. Acad. Sci. U.S.A. **95**, 12799 (1998).
[11]J. J. Timoneda and J. T. Hynes, J. Phys. Chem. **95**, 10431 (1991).
[12]S. Maheshwari, A. Chowdhury, N. Sathyamurthy, H. Mishra, H. B. Tripathi, M. Panda, and J. Chandrasekhar, J. Phys. Chem. A **103**, 6257 (1999).
[13]E. S. Kryachko and M. T. Nguyen, J. Phys. Chem. A **105**, 153 (2001).
[14]O. K. Abou-Zied, R. Jimenez, E. H. Z. Thompson, D. P. Millar, and F. E. Romesberg, J. Phys. Chem. A **106**, 3665 (2002).
[15]A. Ponti and M. Mella, J. Phys. Chem. A **107**, 7589 (2003).
[16]S. Nagaoka, U. Nagashima, N. Ohta, M. Fujita, and T. Takemura, J. Phys. Chem. **92**, 166 (1988).
[17]V. Barone and C. Adamo, J. Chem. Phys. **105**, 11007 (1996).
[18]L. González, O. Mó, and M. Yáñez, J. Phys. Chem. A **101**, 9710 (1997).
[19]J. R. Roscioli, D. W. Pratt, Z. Smedarchina, W. Siebrand, and A. Fernández-Ramos, J. Chem. Phys. **120**, 11351 (2004).
[20]K. Fukuhara, I. Nakanashi, T. Shimada *et al.*, Chem. Res. Toxicol. **16**, 81 (2003).
[21]K. Das, K. D. Ashby, J. Wen, and J. W. Petrich, J. Phys. Chem. B **103**, 1581 (1999).
[22]S. Scheiner, T. Kar, and M. Cuma, J. Phys. Chem. A **101**, 5901 (1997).
[23]E. Bosch, M. Moreno, M. Lluch, and J. Bertran, Chem. Phys. **148**, 77 (1990).
[24]L. Rodriguez-Santiago, M. Sodupe, A. Olivia, and J. Bertran, J. Phys. Chem. A **104**, 1256 (2000).
[25]E. Bosch, M. Lluch, and J. Bertran, J. Am. Chem. Soc. **112**, 3868 (1990).
[26]Z. Smedarchina, A. Fernandez-Ramos, and M. A. Rios, J. Chem. Phys. **106**, 3956 (1997).
[27]A. Fernandez-Ramos, J. Rodriguez-Otero, and M. Rios, J. Chem. Phys. **107**, 2407 (1997).
[28]M. J. Frisch, G. W. Trucks, H. B. Schlegel *et al.*, GAUSSIAN 03, Revision C.02 Gaussian, Inc., Wallingford, CT, 2004.
[29]V. Barone, L. Orlandini, and C. Adamo, Comput. Phys. Commun. **231**, 295 (1994).
[30]V. Barone, L. Orlandini, and C. Adamo, Int. J. Quantum Chem. **56**, 691 (1995).
[31]R. G. Parr and W. Yang, *Density Functional Theory of Atoms and Molecules* (Oxford University Press, New York, 1989).
[32]A. Toro-Labbe, S. Gutiérrez-Oliva, M. C. Concha, J. S. Murria, and P. Politzer, J. Chem. Phys. **121**, 4570 (2004).
[33]B. Herrera and A. Toro-Labbe, J. Chem. Phys. **121**, 7096 (2004).
[34]J. E. Del Bene, S. Ajith Perera, and R. J. Bartlett, J. Phys. Chem. **103**, 8121 (1999).
[35]G. A. Kumar and M. A. McAllister, J. Org. Chem. **63**, 6968 (1998)
[36]S. Scheiner, Y. Gu, and T. Kar, J. Mol. Struct.: THEOCHEM **500**, 441 (2000).
[37]R. D. Parra, S. Bulusu, and X. C. Zeng, J. Chem. Phys. **118**, 3499 (2003).
[38]R. D. Parra, B. Gong, and X. C. Zeng, J. Chem. Phys. **115**, 6036 (2001).
[39]S. Scheiner and X. Duan, *Modeling the Hydrogen Bond* (American Chemical Society, Washington, DC, 1994), pp. 125–138.